



Simple finite element models for use in the design of therapeutic footwear



Thomas A. Spirka^a, Ahmet Erdemir^b, Susan Ewers Spaulding^a, Ann Yamane^a, Scott Telfer^{a,c}, Peter R. Cavanagh^{a,*}

^a Department of Orthopaedics and Sports Medicine, University of Washington, Seattle, WA, USA

^b Computational Biomodeling (CoBi) Core and Department of Biomedical Engineering, Lerner Research Institute, Cleveland Clinic, Cleveland, OH, USA

^c Institute of Applied Health Research, Glasgow Caledonian University, Glasgow, UK

ARTICLE INFO

Article history:

Accepted 13 July 2014

Keywords:

Foot
Model
Finite element method
Diabetes
Footwear

ABSTRACT

Therapeutic footwear is frequently prescribed in cases of rheumatoid arthritis and diabetes to relieve or redistribute high plantar pressures in the region of the metatarsal heads. Few guidelines exist as to how these interventions should be designed and what effect such interventions actually have on the plantar pressure distribution. Finite element analysis has the potential to assist in the design process by refining a given intervention or identifying an optimal intervention without having to actually build and test each condition. However, complete and detailed foot models based on medical image segmentation have proven time consuming to build and computationally expensive to solve, hindering their utility in practice. Therefore, the goal of the current work was to determine if a simplified patient-specific model could be used to assist in the design of foot orthoses to reduce the plantar pressure in the metatarsal head region. The approach is illustrated by a case study of a diabetic patient experiencing high pressures and pain over the fifth metatarsal head. The simple foot model was initially calibrated by adjusting the individual loads on the metatarsals to approximate measured peak plantar pressure distributions in the barefoot condition to within 3%. This loading was used in various shod conditions to identify an effective orthosis. Model results for metatarsal pads were considerably higher than measured values but predictions for uniform surfaces were generally within 16% of measured values. The approach enabled virtual prototyping of the orthoses, identifying the most favorable approach to redistribute the patient's plantar pressures.

© 2014 Elsevier Ltd. All rights reserved.

1. Introduction

Therapeutic footwear is often prescribed to redistribute plantar pressures and attenuate peak pressures in at-risk regions of the foot both to relieve pain in the case of patients with rheumatoid arthritis and to reduce the risk of plantar ulcers in patients with diabetes (Hennessy et al., 2012; Boulton et al., 2004). However, very few guidelines exist as to how these interventions should be designed and what effect such interventions actually have on the plantar pressure distribution (Waaijman et al., 2012). In addition, how footwear designs can be individualized to accommodate patient-specific foot anatomy is not clear. Frequently, the design

of an intervention is based on the clinical experience of the podorthist.

Finite element analysis has the potential to assist in the design process by allowing the clinician to evaluate the effectiveness of many different interventions in order to identify which solution could provide the greatest benefit to a given patient, without having to actually build and test each modification. Several authors have proposed the construction of detailed foot models that incorporate as many of the structures of the foot as possible (Franciosa et al., 2012; Qiu et al., 2011; Hsu et al., 2008; Cheung and Zhang, 2008; Actis et al., 2008) for the purpose of designing footwear. However, development of a full-foot patient-specific model can be a labor-intensive and time-consuming process which frequently results in a computationally expensive model. This limits the feasibility of utilizing models in a translational sense, for a large number of patients and for the often iterative process of footwear design. Simplified two-dimensional models of

* Corresponding author at: Department of Orthopaedics and Sports Medicine, University of Washington Medical Center, Room BB1065D/Box 356500, 1959 NE Pacific Street, Seattle, WA 98195, USA.

E-mail address: cavanagh@uw.edu (P.R. Cavanagh).

the foot with somewhat limited loading conditions have been proposed by Yarnitzky et al. (2006). The goal of the current work was to determine if a simplified 3D model customized for gross patient-specific anatomy could be used to assist in the design of footwear interventions to reduce plantar pressures at targeted forefoot regions. The approach is illustrated by a case study of a diabetic patient experiencing high pressures and pain under the fifth metatarsal head and elevated pressure under the first metatarsal head.

2. Methods

2.1. Finite element representations of the metatarsal region of the foot

Computed tomograms (CTs) of the left foot were acquired with approval of the University of Washington Institutional Review Board from a 46 year-old male (height=1.8 m, weight=74 kg) with Type I diabetes. He presented with callus under

the 1st and 5th metatarsal heads, pain under the 5th despite dense peripheral neuropathy, and a plantarflexed 1st ray. Images were acquired on a GE Lightspeed VCT (GE Medical Systems, Milwaukee, WI) with a slice thickness 0.625 mm. Image resolution was 512 pixel × 512 pixel with pixel size of 0.6 mm × 0.6 mm. The image processing software Scan IP (Simpleware Ltd, Exeter, UK) was used to acquire the measurements listed in Table 1. Briefly, the minimum tissue thickness beneath each metatarsal head (MTH), the length of each metatarsal bone, the maximum width of each MTH, the distance between the center point of each MTH relative to the neighboring MTH and the angle the metatarsal bone made with a straight line running tangent to the plantar surface were all measured. The accuracy and reliability of the above measurements is observer-dependent: for example, five repeat measurements of tissue thickness under MTH2 and the width of MTH2 made by two observers resulted in mean values that differed by less than 0.1 mm and 0.5 mm, respectively, but the coefficients of variation for the two observers were 1%/3% and 5%/11% (observers 1 and 2, thickness/width).

Measurements of gross metatarsal anatomy and tissue thickness were incorporated into a finite element model of the metatarsal region of the foot that utilized simple shapes to represent the bones and the surrounding tissue utilizing Abaqus CAE Version 6.10 (Simulia, Providence, RI). The metatarsal bones were modeled as rigid structures using a combination of a cylinder and a sphere (Fig. 1a). The diameter of the sphere representing the metatarsal head was based on the

Table 1
Measurements acquired from CT scan for construction of the simplified model.

	1st Metatarsal	2nd Metatarsal	3rd Metatarsal	4th Metatarsal	5th Metatarsal
Width of MTH (mm)	25	15	13	13	13
Medial(+)lateral(−) distance relative to MTH3 (mm)	41	17	0	−15	−35
Anterior(+)posterior(−) distance relative to MTH3 (mm)	0	0	0	−10	−23
Thickness of tissue under MTH (mm)	8*	14	10.5	8.5	6.5
Angle relative to plantar surface (°)	30	29	25	23	22
Length of MTH (mm)	64	73	74	77	74

* Average thickness underneath the lateral and medial sesamoids

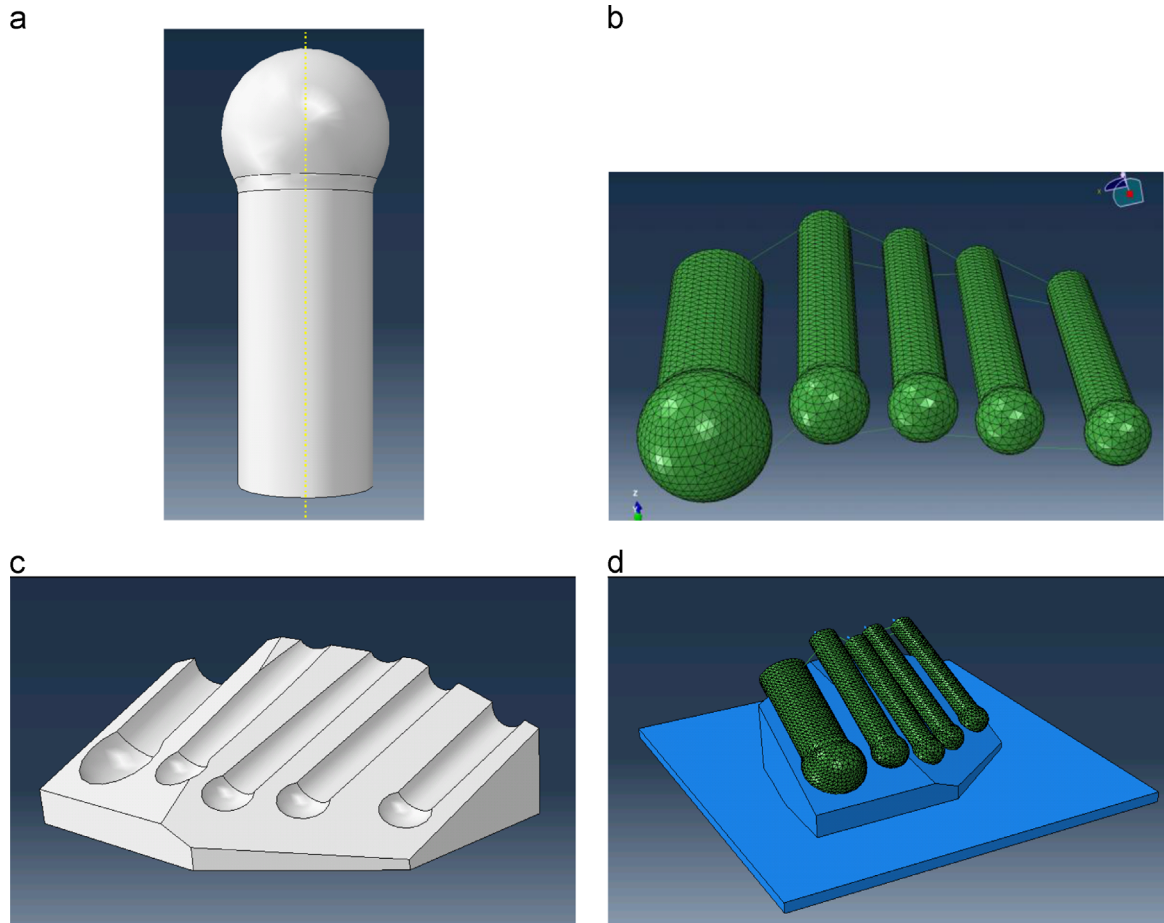


Fig. 1. Model design and construction: (a) simplified shapes used to define the metatarsal bones. (b) Bone orientation showing relative position and angle relative to the plantar surface. (c) Geometry of the soft tissue block. (d) Final model illustrating the barefoot condition.

maximum width of each metatarsal head measured using the CT scans. The overall length of the metatarsal was determined from measurements acquired from the CT scans while the shaft of the bones were assumed to be cylindrical with a diameter equal to 80% of the metatarsal head diameter. The metatarsal bones were then oriented relative to the center point of the third metatarsal head. Finally, the bones were rotated about an axis running perpendicular to the long axis of the bone and through the center point of the spherical metatarsal head to match the angle of the bones observed in the CT scans when the plantar aspect of the foot was parallel to the ground plane. The resulting bone positions can be seen in Fig. 1b. Observation of the patient's barefoot plantar pressure, which showed that peak MTH pressure occurred very soon after heel raise, confirmed this approximation for the MT angles of this model.

Ligaments were incorporated into the model to accommodate restraints on mediolateral splay of the metatarsals. Tension-only truss elements, having elastic material properties ($E=260$ MPa, Poisson's Ratio=0.3) with uniform cross sectional area of (18.4 mm²), were used for this purpose (Cheung and Zhang, 2008). A total of 11 ligament locations were based on the descriptions and drawings provided in Primal Pictures 3D Anatomy Software (Primal Pictures Limited, London, UK). Plantar metatarsal ligaments were attached between adjacent spheres representing each MTH, with attachment points positioned on the plantar surface of the sphere approximately 3 mm medially or laterally from the center axis when viewed in the coronal plane. In a similar manner, plantar and dorsal inter-metatarsal ligaments were attached between adjacent bones approximately 5 mm from the proximal end of the cylinder representing each metatarsal shaft. The connections of the metatarsal bones to the cuneiforms and the cuboid, were modeled using universal joint connector elements (Abaqus 6.10, 2010) to allow for the plantar/dorsiflexion and splay of the metatarsals. The cuneiforms and cuboid were not modeled explicitly but abstracted as a rigid body.

A tissue block (Fig. 1c) was modeled as a nearly incompressible Ogden hyperelastic material ($\mu=0.01645$ MPa, $\alpha=6.82$, effective Poisson's Ratio=0.49, Erdemir et al., 2006). The block was defined such that the plantar surface of the bones were embedded within the block. To accommodate the presence of the metatarsal bones within the soft tissue, Boolean subtraction was used to remove a volume in the shape of metatarsals from the tissue block. Tie constraints between the metatarsal bone surfaces and the surrounding tissue were defined. The arch of the foot was assumed to have an ellipsoidal shape that was defined by the navicular height (13 mm) together with anterior-posterior (152 mm) and medial-lateral measurements (75 mm) of the arch taken from the CT images. This ellipsoidal shape was then Boolean-subtracted from the tissue block to define the arch of the foot. The final resulting model of the metatarsal region of the foot can be seen in Fig. 1d. The soft tissue and bones were meshed using standard linear tetrahedral elements (C3D4) with a characteristic length of 1.8 mm (Cheung and Zhang, 2008; Isvilanonda et al., 2012). A convergence analysis showed that reducing the characteristic element length by 50% resulted in <5% changes in the predicted contact pressures. In addition, a preliminary analysis using nearly incompressible tissue properties (as stated above) illustrated that the predictive capacity for internal and external tissue mechanics metrics were similar to that of a tetrahedral element with hybrid formulation (C3D4H), (the average difference in contact pressures was ~7 kPa). Previously, Tadepalli et al. (2011) have shown the adequacy of tetrahedral elements with hybrid formulation for simulation of nearly incompressible tissue behavior. The element selection used in the present study provided significant cost savings in computational time (~2.5 times faster). The bones were modeled as rigid elements to save computational cost.

As the structures distal to the MTHs were not modeled, the margins of the soft tissue block were constrained to prevent non-physiological motion of the model. The bones were constrained by defining an encastre boundary condition on the posterior reference point of the universal joint element defined for each metatarsal. This resulted in constrained translations and rotations at one end of the tarsometatarsal joints where the rigid body movements of the metatarsals were defined by the universal joint element. The initial model was designed to simulate the barefoot condition by placing the plantar surface of the model in contact with a rigid structure representing the floor that was fully constrained against translation or rotation. Contact at the foot–floor interface was defined by a static coefficient of friction of 0.5.

The model was loaded by applying a concentrated force load to the node closest to the plantar surface of each metatarsal head. To determine the magnitude of each load, the patient walked barefoot at a self-selected speed using a first step protocol across an EMED pedography platform (Novel GMBH Munich Germany) with 4 sensors/cm². The amount of force exerted under the metatarsal heads at the time point corresponding to peak pressure in the gait cycle was determined by integrating pressure over the region of interest. The loads were then modified by inspection based on the resulting predicted plantar pressures until the predicted maximum pressure under each metatarsal head matched the maximum measured pressures in the corresponding region as closely as possible. Once determined, this loading was also utilized for simulations of footwear interventions as described below. Peak regional pressures were obtained from the model output by identifying the largest pressures in a circular region centered on the MTH that did not interfere with adjacent regions.

2.2. Footwear interventions

Prior to the modeling effort, an experienced certified prosthetist/orthotist (CPO) worked with the subject to design personalized footwear that would reduce the plantar pressure at locations determined by the plantar pressure system. In-shoe plantar pressure data was gathered as the participant walked at a self-selected speed over level ground in his shoes and in the various interventions used. The CPO did not have access to model results but was unconstrained in her use of materials or geometries.

To determine the ability of the model to predict the effect of footwear interventions on peak plantar pressures under the metatarsal heads, two types of common footwear interventions designed to reduce plantar pressures in this region were modeled: (1) flat insoles simulating materials of different hardness; and (2) metatarsal pads to relieve focal pressure by increasing pressure at adjacent pressure-tolerant areas. Unless stated, footwear components were modeled as rectangular blocks 110 mm wide by 100 mm long using Abaqus C3D8 hexahedral elements.

The shoe midsole and outsole were modeled as a 13 mm thick flat block (firm crepe) meshed with hexahedral elements with a characteristic length of 4.3 mm. Flat insoles of uniform thickness were meshed on top of the midsole with hexahedral elements with a characteristic length of 2 mm. A convergence analysis was performed for each footwear component, with meshes deemed to be acceptable when reducing the element length by 50% resulted in changes in contact pressures and von Mises stresses of <5%. Three different insole materials, Microcell Puff® (9.5 mm thick), Poron Cushioning® (6 mm thick) and Medium Plastazote® (6 mm thick) were modeled with the hyperfoam material properties shown in Table 2 (Petre et al., 2006). The midsole was constrained by tying the bottom surface to the top surface of the floor, while the bottom surface of the insole was tied to the top surface of the midsole, resulting in no shear movement between the materials. Contact between the plantar tissue and the insole was defined by a static coefficient of friction of 0.5.

To study the effects of metatarsal pads (MPs) on the plantar pressure, a metatarsal pad 66 mm long, 52 mm wide, and 10 mm at the highest point with 2 mm fillet around its top edge (Fig. 2a) was given the properties of Microcell Puff® and placed on top of a 6 mm thick medium Plastazote® insole in three different orientations (Figs. 2b-d). The MP placements were: (a) 6.5 mm proximal to the center point of MTH3; (b) directly under the center point of MTH3; (c) 10 mm lateral to MTH3 to simulate an improper placement. In these simulations, the bottom surface of the pad was tied to the top surface of the insole.

The plantar pressure data from most of the models were validated using pressure distributions measured directly from the subject with the EMED platform for barefoot walking and a Pedar in-shoe system (Novel GMBH, Munich, Germany) for the footwear conditions. The different positions of the MP (b and c above) were not measured directly because: (1) the in-shoe sensors did not have sufficient resolution to make a meaningful measurement; (2) considerations of patient safety suggested that only reasonable modifications should be attempted.

3. Results

By modifying the proportion of the total measured load applied to each metatarsal head in the model, a load condition was identified in which predicted barefoot MTH plantar pressures from the model were within 25 kPa of measured values (3%). The final loads applied to each metatarsal head were 304 N, 115 N, 5 N, 30 N, 74 N on metatarsal heads 1–5, respectively. These loads, which resulted in differences of 20 kPa, 7 kPa, 21 kPa, 1 kPa, and 6 kPa between the measured and predicted peak pressures for each of the metatarsal heads, were then applied to all footwear conditions.

Comparisons between predicted results and measured values can be seen for: (a) the barefoot condition in Fig. 3; (b) three different insoles in Fig. 4; and (c) MPs in various locations in Fig. 5. The overall patterns of measured and predicted plantar pressures are most similar in the flat insole conditions although the peak pressures are consistently over-predicted at the MTHs by the

Table 2
Material properties of insole materials (Petre et al., 2006).

	μ_1 (MPa)	α_1	β_1	Thickness (mm)
Microcell Puff®	1.34	28.07	0.06	9.5
Poron Cushioning®	0.620	34.46	0.04	6.0
Plastazote® medium	0.488	26.09	0.07	6.0
Firm crepe	1.086	27.62	0.091	12.7

simulation. The predicted pattern in the case of the MT pad shows similar elevated peak pressures anterior to the MTHs but the model results in a more detailed distribution than is available from the large elements in the Pedar insole. The absolute values of

plantar pressure are much greater in the simulation as a result of the predicted edge effects (see discussion).

A summary of predicted pressure at each MTH is presented in Fig. 6 where the differences between the standard shod condition

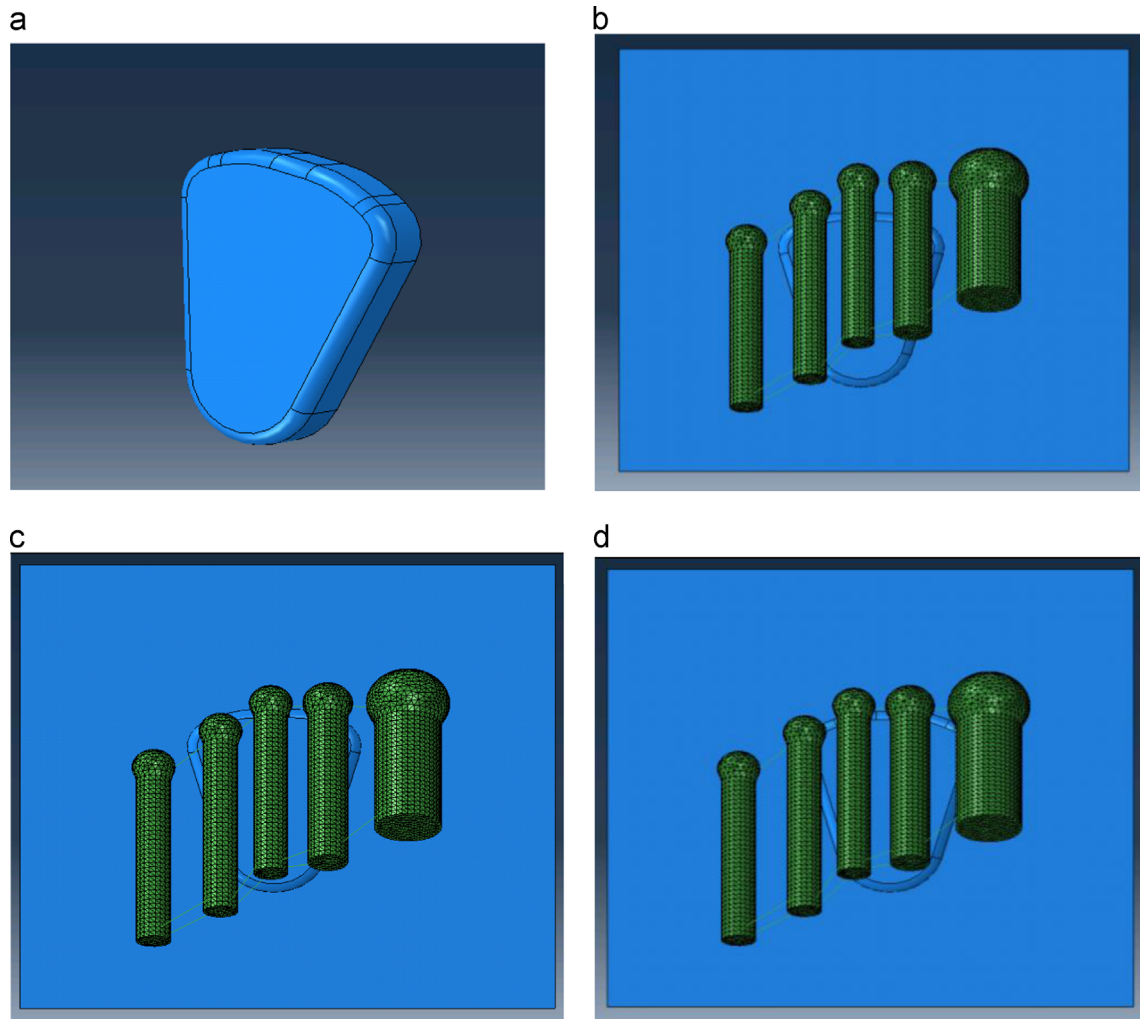


Fig. 2. Modeling of a metatarsal pad: (a) geometry of the metatarsal pad (66 mm long, 52 mm wide, 10 mm at the highest point). (b) Location of the metatarsal pad posterior to the metatarsal heads. (c) Metatarsal pad centered under the 3rd metatarsal head. (d) Improper placement of the metatarsal pad with the pad shifted medially 10 mm from the position shown in (c).

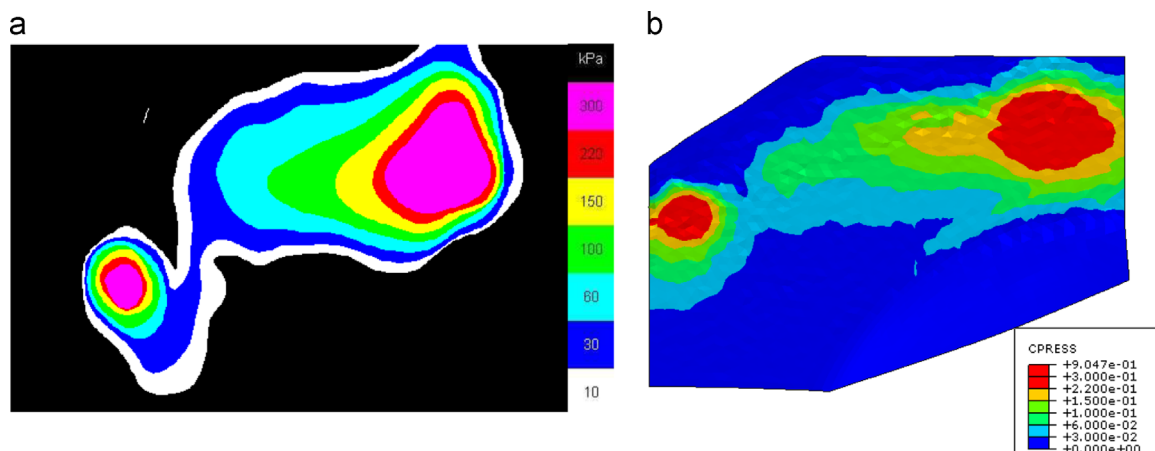


Fig. 3. Comparison of measured (a) and predicted (b) plantar pressure for the barefoot condition. Measured and predicted peak pressure values were 925 kPa and 900 kPa, respectively.

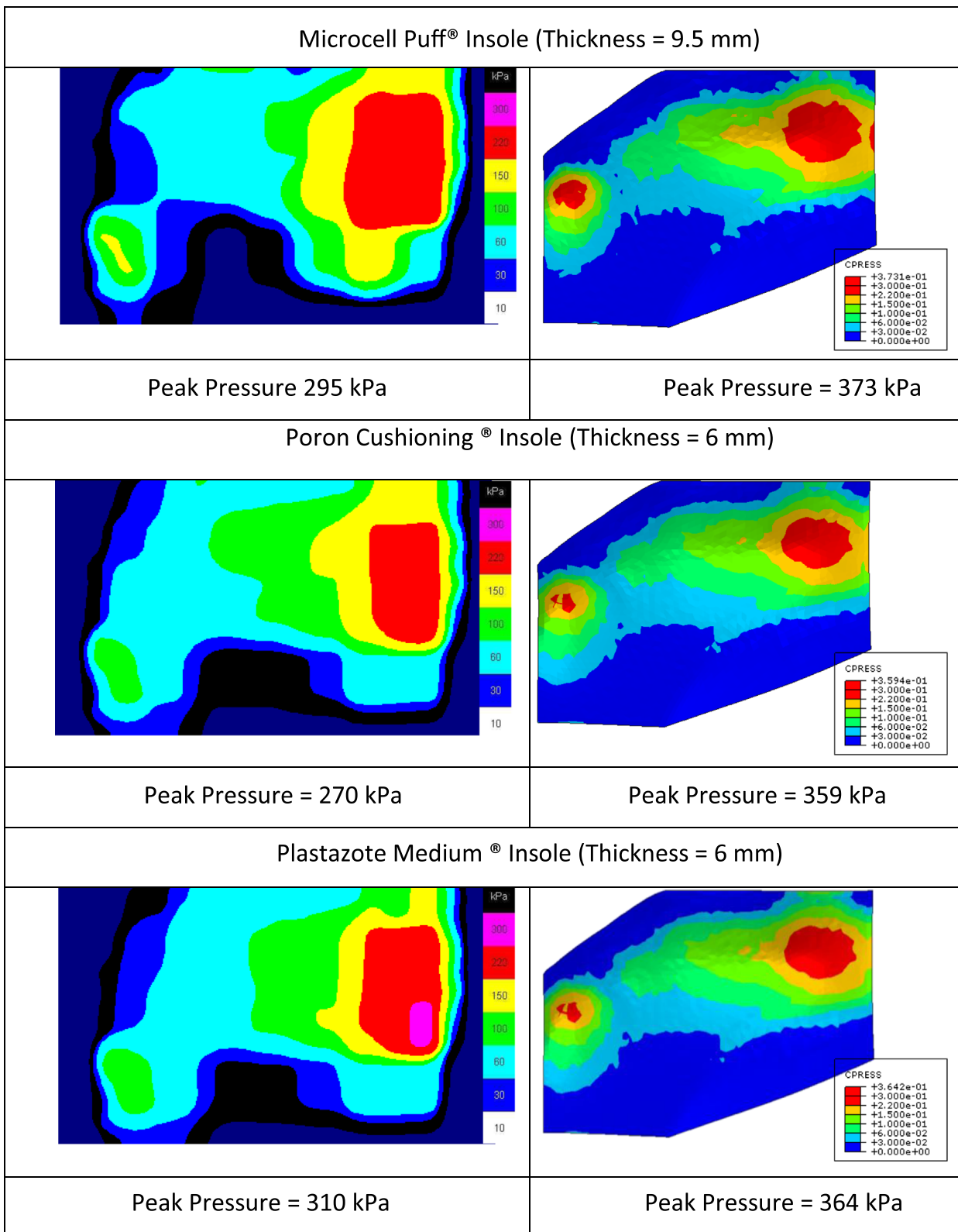


Fig. 4. Comparison of measured (left hand side) and predicted (right hand side) plantar pressure when insoles composed of Microcell Puff® (top), Poron Cushioning® (middle), and Plastazote Medium® (bottom) are incorporated into the model. All three insole materials were successful in reducing the plantar pressure in the region when compared to the barefoot pressure. The Poron Cushioning® insole showed the greatest effect on plantar pressure (both *in silico* and *in vivo*).

and the various interventions are shown in kPa. This figure demonstrates the effect of a given intervention at all MTHs. For example, the proximally placed metatarsal pad (MP condition a) predicted a reduction of peak pressure at MTH1 and MTH5 of

288 kPa and 195 kPa, respectively, but an increase in the peak pressure of 538 kPa, 194 kPa, and 267 kPa at MTHs 2, 3, and 4, respectively. The increases were due to the edge effects shown in Fig. 5b. A more distal placement of the MP was predicted to

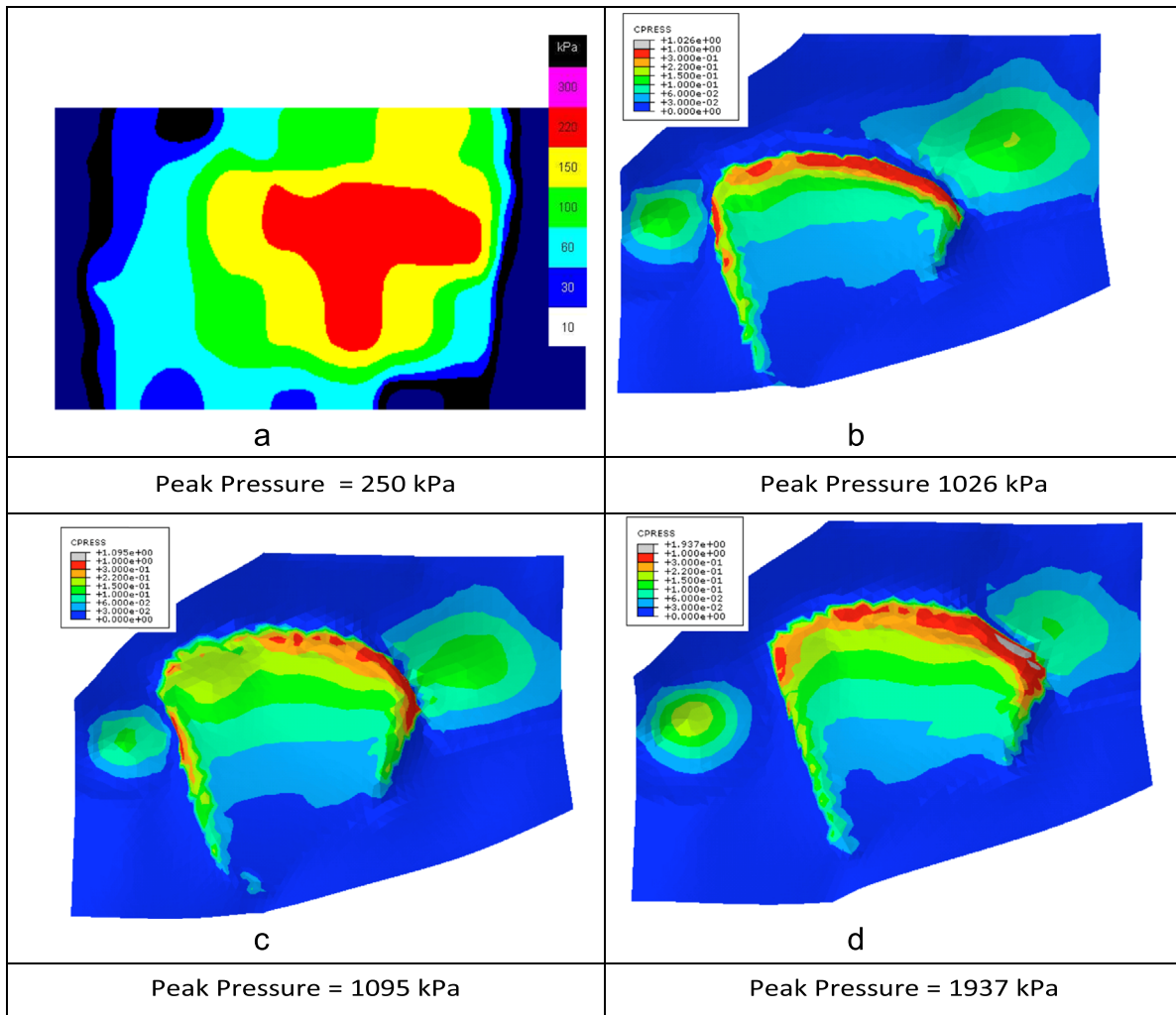


Fig. 5. Effect of incorporating a metatarsal pad on the predicted and measured plantar pressure. (a) Measured plantar pressure when a metatarsal pad was incorporated into the footwear. (b) Metatarsal pad located posterior to the metatarsal heads. (c) Metatarsal pad centered under the 3rd metatarsal head. (d) Metatarsal pad shifted medially 10 mm.

marginally improve offloading at both MTH1 (16 kPa) and MTH5 (33 kPa). Medial placement of the MP reduced offloading at MTH1 (37 kPa) and at MTH5 (56 kPa).

Computational run times using 8 Intel Xeon E5405 CPUs (2 GHz, 40 GB RAM, Windows Server 2003 64-bit OS) varied between conditions with the barefoot model solving the fastest at 14.2 min (wall-clock time) and the MP model the slowest at ~90 min.

4. Discussion

The inherent anatomical and mechanical complexities of the foot makes the task of constructing a model to inform footwear design difficult. This study was intended to test the extent to which a simpler and more economical model could be effective. Such a model needs to characterize key aspects of the patient's anatomy that may affect plantar pressure (Morag et al., 1997) while allowing for multiple iterations of different footwear interventions. Currently, the most common approach is the construction of an FE model of the entire foot based on segmented medical images. However, the necessary procedures required to build such a model are very labor intensive and time consuming. In our experience construction of a single patient-specific foot model can take many weeks and the run times for such models can be several

weeks for a single solution. To overcome these hurdles, we explored the use of simplified models that are still based on patient-specific medical images but which eliminate the need for the labor-intensive and time consuming segmentation and meshing procedures (Cheung and Zhang, 2005). The model still incorporates important parameters that may affect plantar pressures including the thickness of tissue under each metatarsal head, the angle of the bones relative to the plantar surface, bone length, and bone locations relative to one another (Morag et al., 1997). Typical models required only approximately 2 h to build and between 16 min and 90 min to run on commodity computing hardware.

The results demonstrate that this model can reproduce barefoot and in-shoe plantar pressures to within an acceptable degree of accuracy for clinical practice when the interface between the foot and the footwear is relatively simple. For more complex interventions, such as a metatarsal pad, the discrepancies between results measured using a relatively large sensor and a small finite element need to be better understood. The fact that the model estimates of peak contact pressures are larger than the measured values is not surprising since the spatial resolution of the in-shoe measurement system is only $\sim 12 \text{ mm} \times 10 \text{ mm}$ while the individual surface faces of the elements in the model are triangles with initial side lengths of 1.8 mm. Differences in actual vs. modeled soft tissue properties may also have contributed to the difference. The model is also able to detect local areas of stress concentration

(e.g. those associated with the MP in Fig. 5d). This is a frequent clinical concern and a topic that deserves further investigation through simulation since it cannot readily be measured using low-resolution in-shoe sensors.

There are a number of limitations to the present approach. Currently CT or MRI images are needed to establish the model parameters. Further work needs to be done to determine if these values could be obtained using ultrasound, which will enable routine measurements to be made in a clinical setting. The model presented here incorporates several assumptions that are typical of larger models: the soft tissue is modeled as a single lumped tissue layer and represented by a single hyper-elastic material model that is not patient specific. We examined the sensitivity of the plantar pressure results to changes in tissue mechanical properties. A variation of $\pm 25\%$ in ligament properties results only in a $\sim 3\%$ change in peak plantar pressure. Plantar tissue properties were, however, more influential: a variation of $\pm 1\text{ sd}$ in the tissue properties as reported by Erdemir et al. (2006) resulted in a 33% change in the predicted plantar pressure. This large effect emphasizes the importance of using personalized measures of plantar tissue properties in future models. While the incorporation of differentiated tissue layers to allow internal stresses to be accurately predicted (Petre et al., 2013) and viscoelasticity may be feasible, such refinements would significantly increase the labor cost during model development. Viscoelasticity, if modeled, will also increase the computational expense and such adjustments to model fidelity are only needed if research and/or clinical questions dictate their use. The hyperelastic definition used in this model can be justified since the focus is on the response of the tissue for different footwear conditions potentially loaded at a similar rate.

A critical assumption in this model is that the force loading of the metatarsal heads is the same during both barefoot and shod gait –implying that the gait pattern does not change as a result of footwear or the interventions. While this is indeed a limitation, it also established the power of the approach to conduct a predictive analysis of an insole. It is well known that footwear affects the plantar pressures at the foot–shoe interface. However, the relative contributions of footwear and changes in the gait pattern are not known. A further limitation of this model, and the full-foot models published to date, is that only a single instant in time of the gait cycle is considered in the quasi static models, in our case the instant of peak plantar pressure. In reality, the gait cycle is a dynamic event in which the pressures generated and the loads responsible for producing these pressure change continuously. However, the complexity of the foot and the need to reposition structures and alter loads as time evolves hinders development and utility of dynamic models of the foot. Future modeling efforts should also include a more accurate representation of the tarso-metatarsal articulations and their influence on metatarsal orientation.

The metatarsal pad simulations (Fig. 6) highlight how differences in spatial resolution between measured and modeled peak pressure distributions can have a marked effect on the magnitude of the peak pressures. The areas in which focal peak pressures are predicted in the model are only a very small fraction of the area of a single sensor. If such high pressures do exist on the plantar surface of the foot, they will be “averaged” over the entire single sensor area. For this reason, the narrow “ridge” of elevated pressure along the anterior margin of the MP appears in the measured results as a broad row of pressure of considerably lower magnitude. An excellent use of simple models would be to explore the effects of changing the fillet radius of metatarsal pads on the predicted edge

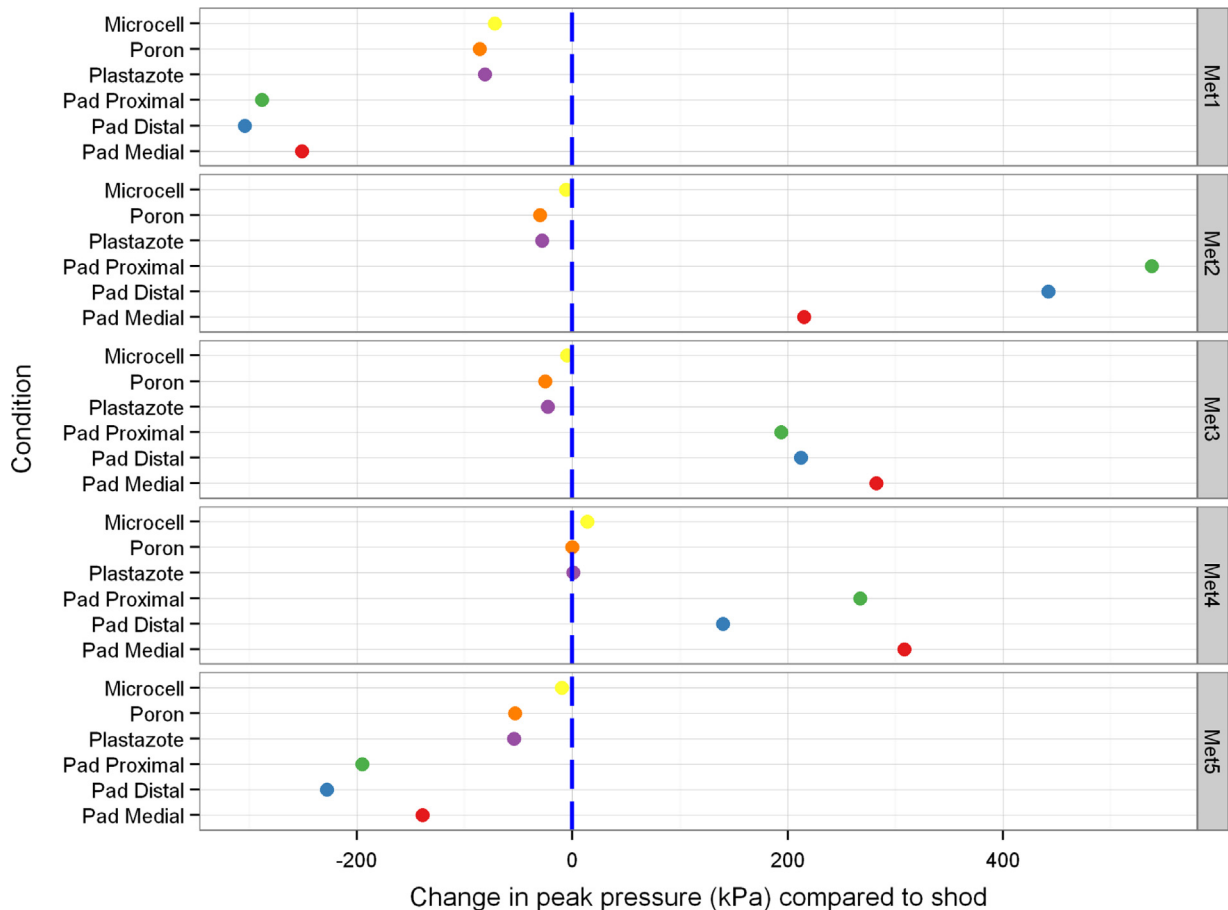


Fig. 6. Predicted change in peak pressure (in kPa) at each MTH for all interventions compared to the standard shod condition.

effects. The origin of the “column” of elevated pressure in the measured MP result may be the narrow ridge of elevated edge effect pressure shown in the simulations along the lateral border of the MP. Although the absolute magnitude and extent of the peak pressure differed markedly between the model and experimentally measured values, the ranking of unloading predicted by different simulations may still be useful in directing clinical attention to the best intervention. Further research to explore the implications of the predicted edge effects is warranted.

5. Conclusions

The proposed work represents a promising approach to the use of FE models in footwear design. Further exploration of the model with more complex footwear interventions and a diverse group of foot types is now warranted. In addition to patient-specific use, the results from a validated model may also find a more general use as a teaching tool for podiatrists to provide insight into the quantitative and qualitative effects of footwear modifications that are typically constructed.

Conflict of interest statement

Peter Cavanagh has equity in DIApacia LLC and Ahmet Erdemir has equity in innodof LLC.

Acknowledgments

This work was supported by NIH Grant 7R01HD037433-08 (PI: Cavanagh). Scott Telfer is funded through the People Programme (Marie Curie Actions) of the European Union's Seventh Framework Programme (FP7 2007–2013) under REA Grant Agreement no. PIOF-GA-2012-329133.

References

- Abaqus 6.10. Abaqus 6.10 User Manual [Internet]. 2010 [cited 2010]. Available from: <http://simulia.com>.
- Actis, R., Ventura, L., Lott, D., Smith, K., Commean, P., Hastings, M., et al., 2008. Multi-plug insole design to reduce peak plantar pressure on the diabetic foot during walking. *Med. Biol. Eng. Comput.* 46 (4), 363–371.
- Boulton, A., Kirsner, R., Vileikyte, L., 2004. Neuropathic diabetic foot ulcers. *N. Engl. J. Med.* 351 (1), 48–55.
- Cheung, J., Zhang, M., 2008. Parametric design of pressure-relieving foot orthosis using statistics-based finite element method. *Med. Eng. Phys.* 30 (3), 269–277.
- Cheung, J.T.M., Zhang, M., 2005. A 3-dimensional finite element model of the human foot and ankle for insole design. *Arch. Phys. Med. Rehabil.* 86 (2), 353–358.
- Erdemir, A., Viveiros, M.L., Ulbrecht, J.S., Cavanagh, P.R., 2006. An inverse finite-element model of heel-pad indentation. *J. Biomech.* 39 (7), 1279–1286.
- Franciosa, P., Gerbino, S., Lanzotti, A., Silvestri, L., 2012. Improving comfort of shoe sole through experiments based on CAD-FEM modeling. *Med. Eng. Phys.*
- Hennessey, K., Woodburn, J., Steultjens, M.P.M., 2012. Custom foot orthoses for rheumatoid arthritis: a systematic review. *Arthritis Care Res.* 64 (3), 311–320.
- Hsu, Y., Gung, Y., Shih, S., Feng, C., Wei, S., Yu, C., et al., 2008. Using an optimization approach to design an insole for lowering plantar fascia stress—a finite element study. *Ann. Biomed. Eng.* 36 (8), 1345–1352.
- Isvilanonda, V., Dengler, E., Iaquinto, J.M., Sangeorzan, B.J., Ledoux, W.R., 2012. Finite element analysis of the foot: model validation and comparison between two common treatments of the clawed hallux deformity. *Clin. Biomech. (Bristol, Avon)* 27 (8), 837–844.
- Morag, E., Pammer, S., Boulton, A., Young, M., Deffner, K., Cavanagh, P., 1997. Structural and functional aspects of the diabetic foot. *Clin. Biomech. (Bristol)* 12 (3), S9–10.
- Petre, M., Erdemir, A., Cavanagh, P., 2006. Determination of elastomeric foam parameters for simulations of complex loading. *Comput. Methods Biomed. Eng.* 9 (4), 231–242.
- Petre, M., Erdemir, A., Panoskaltsis, V.P., Spirka, T.A., Cavanagh, P.R., 2013. Optimization of nonlinear hyperelastic coefficients for foot tissues using a magnetic resonance imaging deformation experiment. *J. Biomech. Eng.* 135 (6), 61001–61012.
- Qiu, T.X., Teo, E.C., Yan, Y.B., Lei, W., 2011. Finite element modeling of a 3D coupled foot-boot model. *Med. Eng. Phys.* 33 (10), 1228–1233.
- Tadepalli, S.C., Erdemir, A., Cavanagh, P.R., 2011. Comparison of hexahedral and tetrahedral elements in finite element analysis of the foot and footwear. *J. Biomech.* 44 (12), 2337–2343.
- Waaijman, R., Arts, M.L.J., Haspels, R., Busch-Westbroek, T.E., Nollet, F., Bus, S.A. Pressure-reduction and preservation in custom-made footwear of patients with diabetes and a history of plantar ulceration. *Diabet. Med.* 2012.
- Yarnitzky, G., Yizhar, Z., Gefen, A., 2006. Real-time subject-specific monitoring of internal deformations and stresses in the soft tissues of the foot: a new approach in gait analysis. *J. Biomech.* 39 (14), 2673–2689.